



Power Electronic Systems  
Laboratory

© 2021 IEEE

Proceedings of the 24th International Conference on Electrical Machines and Systems (ICEMS 2021),  
Gyeongju, Korea, October 31-November 3, 2021

## **Magnetically Self-Bearing Drive System for Ultracentrifugation: Towards 100'000 rpm and 200'000 g**

E. Hubmann,  
C. Blaser  
S. Erismann,  
D. Steinert,  
T. Nussbaumer,  
J. W. Kolar

Personal use of this material is permitted. Permission from IEEE must be obtained for all other uses, in any current or future media, including reprinting/republishing this material for advertising or promotional purposes, creating new collective works, for resale or redistribution to servers or lists, or reuse of any copyrighted component of this work in other works.



Eidgenössische Technische Hochschule Zürich  
Swiss Federal Institute of Technology Zurich

# Magnetically Self-Bearing Drive System for Ultracentrifugation: towards 100'000 rpm and 200'000 g

Emanuel J. Hubmann\*, Christian F. Blaser\*, Stefan Erismann\*, Daniel Steinert†, Thomas Nussbaumer†, Johann W. Kolar\*

\*Power Electronic Systems Laboratory ETH Zurich, Switzerland, hubmann@lem.ee.ethz.ch

†Levitronix GmbH Zurich, Switzerland, steinert@levitronix.com

**Abstract**—A novel magnetically double self-bearing drive system for ultracentrifugation is presented. It features an operating speed of 100'000 rpm, enabling centrifugal acceleration levels of 200'000g. The new drive system uniquely allows simple access to the centrifuge rotor for removal and loading. The design requirements are derived and the system feasibility is proved. The drive system working principle is demonstrated, a self-bearing motor prototype and an according test-system is shown. A control method thereof is proposed and the system resonance behavior is analyzed analytically and with 3D-FEM. An experimental validation of the control strategy on a control system test-platform completes the feasibility proof.

**Index Terms**—self-bearing motor, high-speed, ultracentrifugation, control

## I. INTRODUCTION

In biochemistry, fundamental processes are the separation of components of heterogeneous mixtures and purification with the aid of centrifuges. Typical centrifuge rotors today are mechanically suspended. Mechanical suspension at high speeds sheds light on necessary sealing, bearing losses, lubrication, wear, contamination and limited life-time or maintenance needs. These are all examples of challenges and potential sources of design restrictions of the current technology.

This paper presents a novel magnetically self-bearing drive system, omitting this limitations and offering a unique feature, enabling easy access to the ultracentrifuge rotor or allows for removal of it by the user.

In [1], a magnetic levitation based continuous flow ultracentrifuge (UCF) prototype was presented, reaching a centrifugal acceleration of up to  $C = 10^5g$  and a flow rate of  $Q = 0.4 \text{ L/min}$  with a rotational speed of higher than 64krpm. It uses helium as a surrounding gas to reduce gas friction losses. In this paper, the path towards magnetic levitation in ultracentrifugation is continued and presents a concept for a 100krpm and  $C = 2 \cdot 10^5g$  UCF drive system, incorporating unique features. Fig.1 shows a conceptual illustration thereof. Two self-bearing motors (SBMs), forming a double self-bearing motor DSBM, drive the centrifuge rotor and keep it contactless in place. As a special feature, a joint between the SBM modules allows access to the rotors and simple insertion or

The authors gratefully thank the Swiss Innovation Agency Innosuisse for their financial support and Levitronix GmbH for their financial, scientific as well as technical contributions.

removal thereof.

The drive system consists on the one hand of the hardware and on the other hand of the control system. In magnetic levitation, the control system is of fundamental importance. Therefore this paper focuses on both hardware and control of the proposed drive system concept. Fig. 2 shows a map of the drive system concept development landscape. For a motor concept (Fig. 2a), different motor topologies (Fig. 2b) can be derived and assessed with e.g. 3D-FEM analysis (Fig. 2c). At the core of the development are the requirements (Fig. 2d) which are highly application (Fig. 2f) dependent. Designs can then be scaled along parameters as power or torque (Fig. 2e). The requirements for a self-bearing ultracentrifuge drive system differ quite substantially from other self-bearing motor applications. Fig. 2d shows qualitatively the different priorities for performance parameters in a spider diagram compared to levitated industrial fans (Fig. 2f1) comparable to e.g. [2] and satellite reaction wheels (SRW) (Fig. 2f2) comparable to e.g. [3]- [4].

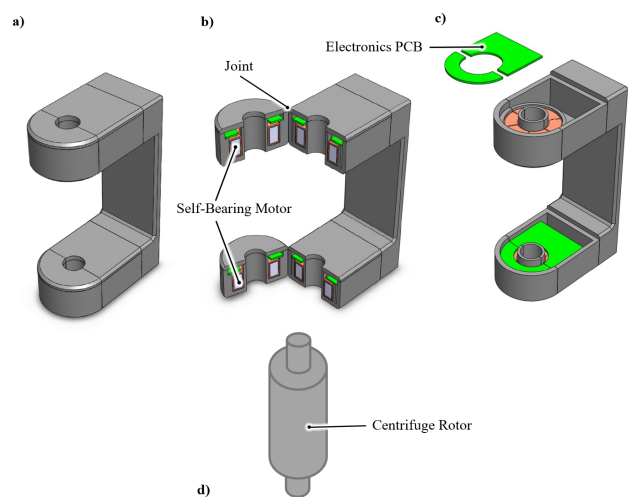


**Fig. 1:** a) Conceptual illustration of a novel magnetically self-bearing drive system for 100'000 rpm and 200'000g ultracentrifugation. b) The proposed motor concept enables easy access for e.g. insertion or removal of centrifuge rotors. c) Possible placement of the power electronics. d) Conceptual illustration of the ultracentrifuge rotor.

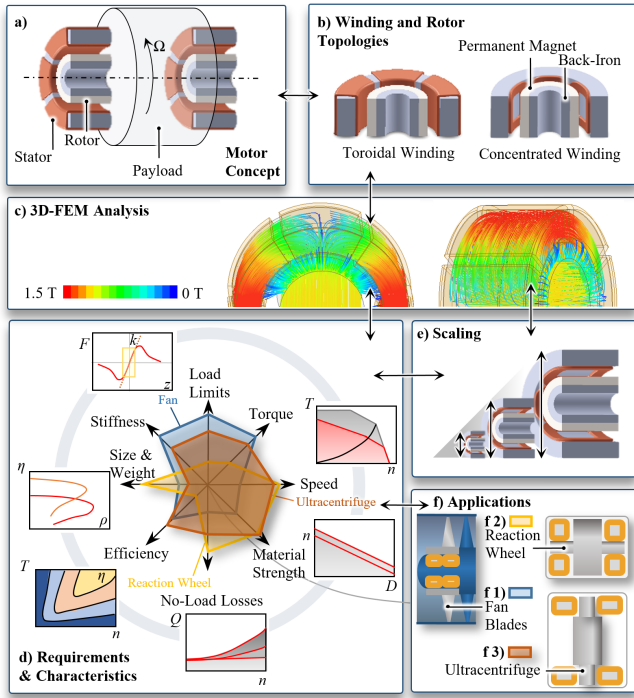


**Fig. 2:** a) Slot-less double SBM concept (DSBM) with b) different winding topologies, c) motor investigations by 3D-FEM. Motor scaling illustration e), comparison of requirement priorities for selected potential DSBM applications displayed in a spider diagram d) for an industrial fan f1), a reaction wheel f2) and ultracentrifugation f3).

It is remarkable, that for UCF SBMs, an especially large area in the requirement domain needs to be covered. Size and weight are the only requirements for UCF SBMs, which are comparably low, as UCFs are typically part of an anyway heavy process unit. For bearing stiffness, load limits and torque demand, UCF SBMs lie somewhere between fans and SRWs. UCFs need very high speeds to achieve high centrifugal accelerations, what directly explains the high material strength requirement. Compared to SRWs, the no-load losses are not directly a criteria, as UCFs constantly need to overcome the gas friction. Still, low no-load losses naturally are needed as the efficiency criteria is very important. It is important because the power demand should not be excessive, and the sensitive process media in the UCF rotor should not be heated by the generated losses. Overall, the requirements for UCF SBMs are tough and position them in the field of high-speed high-performance special machines.

This paper is structured as follows: **Sec. II** identifies the to be targeted performance goals and the feasibility of their realization. In **Sec. III** the novel self-bearing motor concept for ultracentrifugation is discussed. Additionally, a UCF self-bearing motor prototype and an according test-system is presented. **Sec. IV** shows the proposed control structure for the novel ultracentrifuge drive system, a detailed investigation on system resonance phenomena and a successful experimental validation of the control system on a control system test-platform. The findings are finally summarized in **Sec. V** and an outlook is provided.

## II. REQUIREMENTS AND FEASIBILITY

First, the performance goals are investigated to achieve great centrifugation results, in a second step the system feasibility is assessed based on the power demand to overcome the gas friction, and as a third aspect, the feasibility of the UCF rotor in terms of mechanical strength is investigated, as it is the highest mechanically loaded system component.

### A. Centrifugation Performance

In centrifuges, separation is driven by density difference induced sedimentation of mixture components. This process is accelerated in centrifuges by drastically increasing the force field. From Stokes law it follows that the sedimentation rate is proportional to the relative centrifugal acceleration  $C$ , i.e. the relative centrifugal acceleration w.r.t earth's gravity  $g = 9.81 \text{ ms}^{-2}$  [5]. Additionally the centrifuge working principle, shape, volume and dimensions influence the outcome. Centrifuges can be distinguished into discrete volume or continuous flow centrifuges. Continuous flow centrifuges have the advantage of reducing cost and time for larger process quantities [5]. The performance of continuous flow centrifuges can be compared with e.g. the g-volume approach [8]. Similar centrifugation results can accordingly be expected if the product of  $C$  value and centrifuge rotor volume  $V$  divided by the flow rate  $Q$  stays constant.

$$\frac{C_i \cdot V_i}{Q_i} = \text{const.} \quad (1)$$

$C$  can be expressed as

$$C = \frac{r \cdot \Omega^2}{9.81 \frac{\text{m}}{\text{s}^2}} \quad (2)$$

and is therefore proportional to the radius  $r$ , and to the squared mechanical angular frequency  $\Omega$ . Processes with  $C$  values of approx.  $10^5 g$  and larger are referred to as ultracentrifugation [5]. Therefore very high speeds and radii are desired for UCFs, resulting in  $C$  values larger than  $10^5 g$ . This design requirements are associated with design challenges. Increasing speed and radius leads to higher gas friction losses and thus power demand and increases the centrifuge rotor material stresses.

### B. Power Demand

In this paper, the maximum electrical input power to the DSBM, i.e. the max. output power of the power electronics is chosen to be 1 kW for a laboratory scale prototype design. This decision defines a loss budget of 0.5 kW per individual SBM. **Fig. 3a** shows the air friction losses for an UCF rotor with a gap between casing and rotor of  $\delta = 1 \text{ mm}$  and centrifuge rotor radii from  $r_o = 1 \dots 3 \text{ cm}$  based on the experimentally determined correlations for Taylor-Couette flow reported and discussed in [6], [7]. An air friction loss of approx. 600 W for an rotor radius of  $r_o = 3 \text{ cm}$  and rotor length of 10 cm is regarded in this paper to be reasonable, given the total loss budget of 1 kW. The additional 0.4 kW can be distributed for

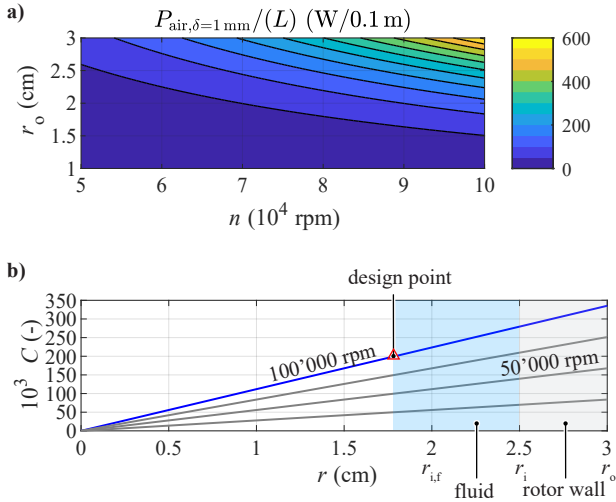


**Fig. 3:** a) Air friction losses  $P_{\text{air}}$  of a rotor enclosed in a stationary cylindrical casing per length  $L = 10$  cm depending on speed  $n$  and rotor radius  $r_o$ . b) achievable relative centrifugal acceleration depending on rotational speed and rotor radius, including the envisaged design point (inner fluid radius).

SBM and continuous centrifuge supply flow losses. **Fig. 3b)** reveals, which maximum relative centrifugal acceleration  $C$  can be achieved, depending on the inner rotor i.e. outer fluid-radius  $r_i$ . Additionally, depending on the inner fluid radius  $r_{i,f}$ , the average centrifugal acceleration for all fluid in the centrifuge rotor will be lower, but beneficially the centrifuge fluid-volume is increased. The combination can be chosen to suit best a given centrifugation task. **Fig. 3** proves, that with 1 kW and 100'000 rpm, and a centrifuge rotor radius of 3 cm, relative centrifugal accelerations of 200'000g and higher can be achieved.

### C. Mechanical UCF Rotor Strength

The mechanical strength of the UCF rotor needs to be high enough to withstand the stresses occurring during operation. **Fig. 4** shows the stress distribution in a stainless steel (304 1.4301) rotor wall rotating at 100'000 rpm, taking into account the pressure on the inner wall due to the co-rotating fluid (water). The stress distribution was analytically calculated based on [9] and the fluid pressure influence based on [10]. **Fig. 4a)** shows the stresses for a partially and **Fig. 4b)** for a fully filled rotor. The highest stresses occur at the inner rotor wall  $r_i$ . The circumferential stress  $\sigma_c$  dominates, such that the equivalent stress  $\sigma_v$  is almost identical to the circumferential stress. The comparison of **Fig. 4a)** and **Fig. 4b)** shows a small but significant increase in circumferential stress, if the rotor is fully filled with fluid. For the evaluation of mechanical strength, the material choice is central. Density, strength and fatigue behaviour determine the material performance. A drastic impact has the decision on the number of operating cycles which the system should withstand [11]. If the design is allowed to have a limited life-time or operating cycles, the admissible stresses are higher, compared to a design with unlimited (i.e. not specified) life-time. **Fig. 5** shows based on

the same analytic approach, which materials are strong enough to withstand the stresses occurring in the envisaged centrifuge design of **Fig. 3b)**. Both aluminum and steel can only provide very limited life-time. Titanium can provide an unlimited life-time. Carbon fibers as well, though carbon fibers would be applied as a bondage on a base rotor material. Therefore the ultracentrifuge concept is feasible and reaches with 100'000 rpm centrifugal accelerations of higher than 200'000 g with a loss budget of 1 kW. It was shown that the UCF rotor can be designed with available materials. The focus can therefore be brought to the UCF SBM drive system.

### III. SELF-BEARING MOTORS FOR UCFs

Self-bearing motors (SBMs) have the unique capability of taking over both the driving and magnetic bearing functionality. This beneficially simplifies the drive system architecture, as no separate magnetic bearing units next to the motors are required.

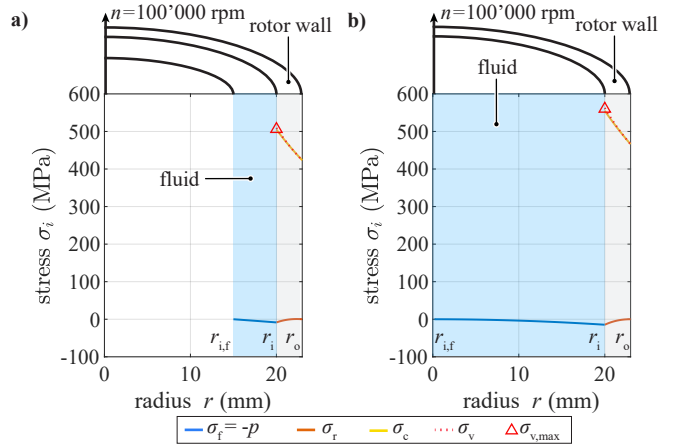


**Fig. 4:** Stress distribution in a rotating stainless steel 304 1.4301 cylinder rotating at 100'000 rpm, a) partially and b) fully filled with water. The highest equivalent  $\sigma_{v,max}$  stress occurs on the inner cylinder wall surface.

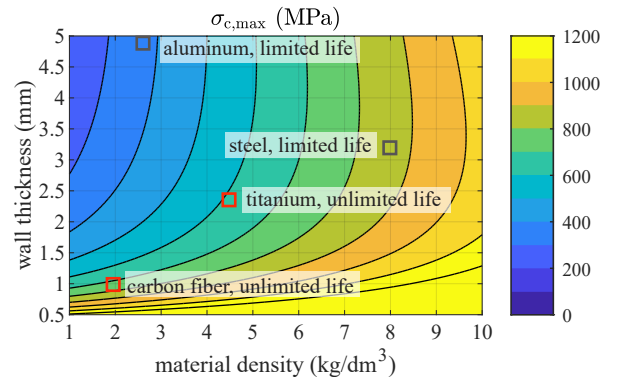


**Fig. 5:** Material performance feasibility in terms of strength, life-time and required UCF rotor wall thickness for the proposed ultracentrifuge design with respect to the maximum circumferential stress  $\sigma_{c,max}$ , resulting from using those materials. For aluminum and steel, only limited life time can be achieved. For titanium and carbon fiber (rotor bondage), unlimited life can be achieved.

### A. Working Principle

In **Fig. 6** the working principle for SBM torque **a)** and force generation **b)** is shown. In SBMs, drive and bearing currents create fields in the same air-gap. The magnetic bearing forces can either be generated with the aid of separate bearing windings, or with the aid of a mathematical superposition of bearing and drive currents in so-called combined windings, as shown in e.g. [13] and employed in this paper. The stator field and related forces acting on the rotor are created by superimposed currents of drive and bearing action as shown in e.g. [16]. For the torque generation, in **Fig. 6a)**, a stator field with the same pole-pair number as the rotor is generated commonly with all six windings. It is  $90^\circ$  ahead of the rotor permanent magnet field, which leads to a torque generation. To create bearing forces as shown in **Fig. 6b)**, the same six windings generate a two-pole pair stator field which generates together with the rotor field bearing forces with arbitrarily controllable amplitude and direction.

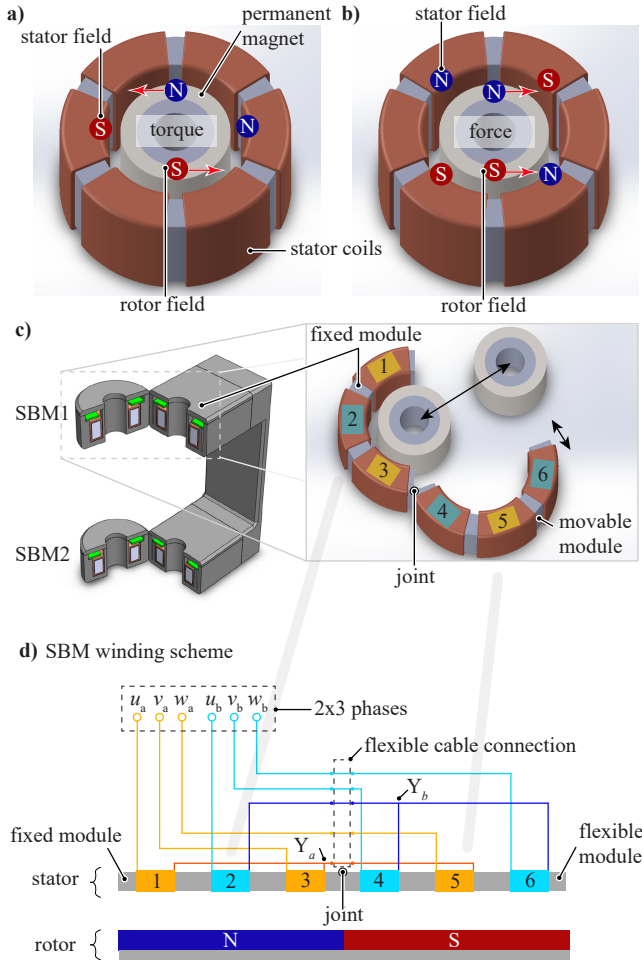


**Fig. 6:** Working principle of the slotless SBMs for driving torque **(a)** and bearing force generation **(b)**. **(c)** Opening stator capability of the proposed UCF SBMs enabling access and removal of the UCF rotor. **(d)** SBM winding scheme of the proposed topology.

### B. Topology for UCF SBMs

For the UCF application, the topology of slotless SBMs with combined windings in toroidal realization as shown in **Fig. 6c)** exhibit several advantages. First of all, it allows for a separation of the stator in two stator modules, enabling the opening of the movable SBM module like a door with a mechanical joint for easy access and removal to the UCF rotor. Generally the windings can be placed in slots of a motor's stator core or being exposed directly to the air-gap magnetic field in a slot-less design. The realization with a slotless stator leads to lower losses for very high speeds. The higher losses of slotted designs are caused by stronger and higher order harmonics in the air-gap field due to the teeth interaction with the field [14]. A slight disadvantage is, that slotless SBM designs show generally a lower bearing stiffness compared to slotted designs [12], but for UCFs the stiffness requirements are lower compared to e.g. pumps and fans, therefore this is not a contradiction to the topology choice. Slotless SBMs can exhibit an almost sinusoidal air-gap field for the rotor pole-pair number  $p = 1$  [15], which is ideal for highspeed applications. It results in very low harmonic field content and  $p = 1$  leads to the lowest possible fundamental electrical frequency for a given mechanical speed, resulting again in low losses. Therefore for UCF SBMs, a slotless topology with pole pair number equal to one seems to be very promising. Using combined windings for bearing forces and torque generation, leads to equal loading of all windings and always full utilization of the winding copper cross-section. If the bearing currents would be active in separate bearing coils, that would not be the case. Therefore also all semiconductors of the connected power electronics, feeding those windings benefit from equal current loading as well. Additionally, in [15] it was shown that the usage of combined windings lowers the higher order field harmonics induced by the stator drive and bearing currents, reducing the current induced losses at high speeds.

In **Fig. 6d)** the winding scheme of the resulting SBMs topology is presented. It consists of two three phase systems  $a$  and  $b$  with phase connections  $u_a, v_a, w_a$  and  $u_b, v_b, w_b$  respectively. The two three phase systems are star-connected at the star-points  $Y_a$  and  $Y_b$  respectively. The connection between the two modules is established by flexible cable connections. By transferring three phase and two star-point lines from the fixed module to the flexible one, the SBM stator winding with opening capability is fully connected.

A further advantageous property of the proposed UCF drive system topology is the fact, that in axial direction the SBMs are passively stable due to the attractive forces of the rotor permanent magnet to the stator core. Additionally, tilting is stabilized by actively controlling the radial position of both SBMs.

### C. UCF SBM Prototype and Testsystem

**Fig. 7** shows a realized  $48 V_{DC}$  fed  $0.5 kW$  SBM prototype of the previously discussed topology for UCF application, installed on a UCF SBM test system. It is powered by

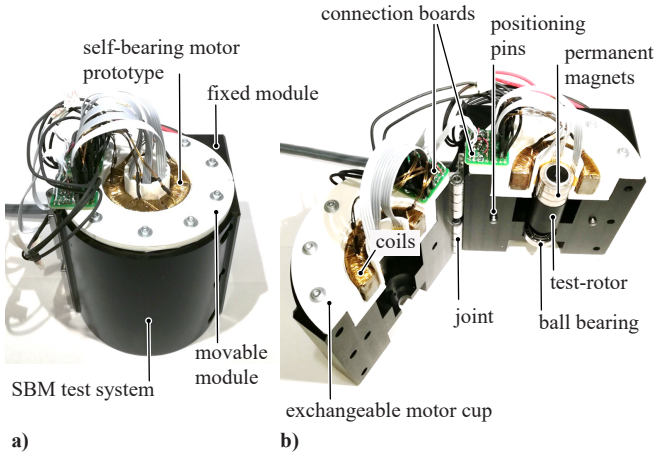


**Fig. 7:** Realized UCF SBM prototype integrated into a purpose-built SBM test system. The test system is closed during operation (a) and can be opened like in the targeted UCF application for easy access or rotor exchange (b).

a two times three phase inverter mounted on the rear of the test system. The test system consists of a fixed and a movable module connected with a joint, allowing for opening of the motor. Positioning pins enable precise alignment of both modules. Two connection boards enable connecting the motors and modules. Removable motor cups allow for testing of different SBM prototypes. To facilitate commissioning of the SBM, the lower end of the test-rotor features a high-speed mechanical ball bearing. This enables commissioning of one single SBM. To omit the mechanical bearings, in a next step two SBM are needed. The employed ball bearing is a high-speed bearing, but still limits the maximum speed to approximately 70'000 rpm. Higher speeds require a fully operational system of two SBM combined to a DSBM and a control system.

#### IV. CONTROL STRUCTURE AND EXPERIMENTAL VERIFICATION

A big part of the success of a high-speed magnetically levitating drive system is its control system. To investigate and verify control strategies and algorithms for UCF DSBM drive systems, the drive system control test-platform shown in **Fig. 8** was established. It consists of two opposing 20'000 rpm SBMs and a test-rotor. The individual SBMs are realized in temple architecture [16], which differs from the slotless design of the UCF SBMs. But since both SBMs generate a bearing stiffness, the system behavior and thus the needed control algorithms are in principle the same and can therefore be investigated on the control test-platform SBMs as well.

##### A. Control Structure

**Fig. 9** shows the proposed UCF DSBM drive system control structure. It is designed as a decentralized control structure. This allows direct integration of the power and control electronics into each SBM housing. Both SBMs control their radial rotor position independently with a cascaded position control loop. An additional force-rejection algorithm

as described e.g. in [17] reduces the power consumption and bearing forces due to rotor imbalance. For the speed control, one SBM is assigned a master role, and the other a slave role. The speed control is conducted on the digital signal processing unit (DSP) of the master only. It is designed as a cascaded control loop as well. The reference torque is sent from the master via a CAN-bus to the slave, which only has the drive current loop part of the speed control. With this concept, the two SBMs and their power and control electronics can be built identically and simply connected with a DC power bus and a CAN data bus. This architecture has the potential to reduce development, manufacturing and product cost. To verify the functioning of the proposed UCF DSBM drive system control structure, it was implemented on the control test environment shown in **Fig. 8**.

For the control system, especially resonance frequencies of the DSBM system are critical to stabilize. On the one hand the interaction of bearing stiffness together with the rotor inertia and rotordynamics are one source of resonances. Another source can be the bending resonances of the rotor. To judge how well the proposed control method works, the resonance frequencies of the test-platform DSBM system are investigated in the following.

##### B. Rotor Rigid Body Modes

One kind of vibration modes which can lead to system resonances are the rigid body modes. They are analyzed in the following analytically and with a three dimensional finite element method (3D-FEM). The responsible stiffness contributor for these modes is the magnetic bearing stiffness  $k_B$ , i.e. the radial force on the rotor of one SBM ( $F_r$ ) per radial deviation ( $r$ ).

$$k_B = \frac{-F_r}{r} \quad (3)$$

The rotor mass and its moments of inertia provide the needed inertia.  $k_B$  is a function of the magnetic interaction between stator and rotor. Passive magnetic forces due to the attraction of the rotor permanent magnet to the stator core acts in the present system destabilizing in radial direction but stabilizing

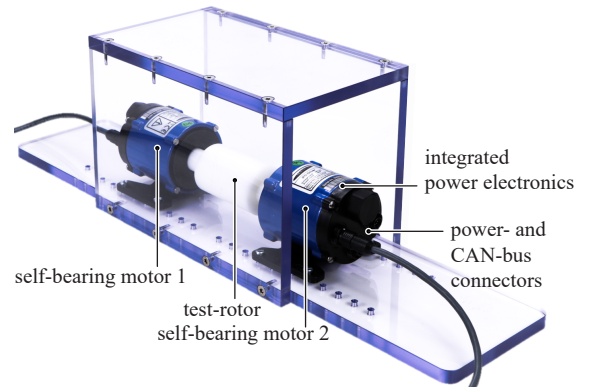


**Fig. 8:** Realized 20'000 rpm double self-bearing motor drive system control test-platform.

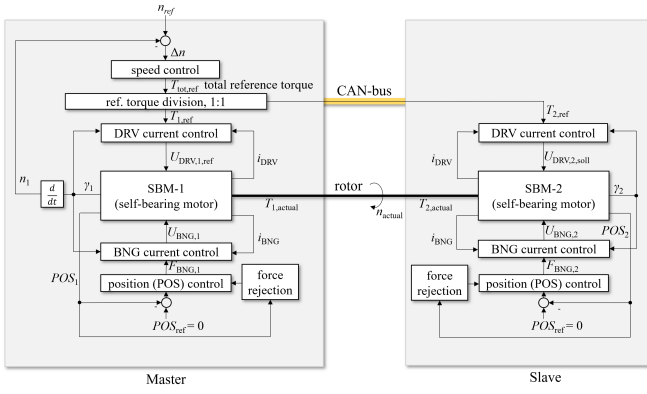


**Fig. 9:** Decentralized control structure of the proposed DSBM system, the two SBMs control their rotor position (POS) with magnetic bearing (BNG) action independently. A speed ( $n$ ) control loop with torque ( $T$ ) distribution to both SBMs ensures combined driving (DRV) effort.

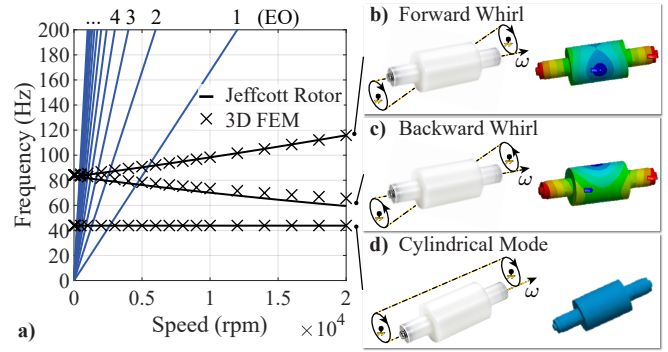


**Fig. 11:** This figure shows the rigid body modes of the test-rotor. a) Campbell diagram with Jeffcot and 3D FEM rotor model results of the rigid body modes. The excitation orders (EO) 1-12 are indicated as well. The principal motion and corresponding FEM results for the displacement pattern from the initial position (blue=low, red=high) for the forward whirl b), backward whirl c) and cylindrical mode d) are shown.

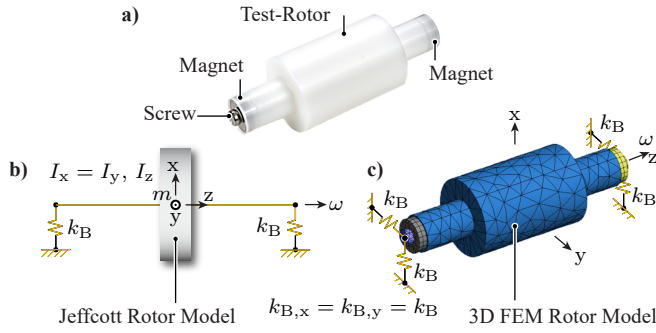


**Fig. 10:** a) Test-rotor with two diametrically magnetized permanent magnets and corresponding stainless steel screws, fixing the magnet portion to the test-rotor. b) Jeffcott rotor model with flexible bearings with bearing stiffness  $k_B$  and a rigid shaft. A rigid Disk with moments of inertia  $I_x$  and lumped rotor mass  $m$  is placed at the middle of the shaft. c) 3D FEM model of the rotor.

in axial direction. The radial rotor position needs to be actively stabilized with the bearing coils. The radial bearing stiffness is therefore hardware and control algorithm dependent. For this reason,  $k_{B,r}$  was determined experimentally by measuring the deflection of the rotor due to its own weight with the SMBs onboard position sensing system, while any integrating action of the position controller was turned off.  $k_{B,r}$  resulted in 5.6 N/mm.

**Fig. 10a)** shows the control test-platform test-rotor. It consists of a 40 mm thick cylinder made out of POM-C, diametrically magnetized permanent magnets (PMs) and stainless steel screws, which hold the attached PMs in place. As an analytic rotor model to predict the rotor rigid body modes, the Jeffcott rotor model shown in **Fig. 10b)** was employed. The rotor mass  $m$  is lumped to the center of the rotor. The moments of inertia  $I_x, I_y$  and  $I_z$  are lumped as well, giving the model parameters for a rigid disk. The shaft was assumed to be rigid and massless. **Fig. 10c)** shows the established 3D-FEM rotor model. In the following, the results of both models for the rotor rigid body modes are presented and compared.

Three rigid body modes were derived and computed according to [18] and confirmed with 3D-FEM modal analysis including

rotor dynamic effects: a cylindrical mode, where the rotational axis always keeps direction, and two conical modes, a backward and a forward whirl, shown in **Fig. 11b)-d)**. In **Fig. 11a)** both analytic and FEM results for the corresponding resonance frequencies are shown in a Campbell diagram, including the excitation orders (EOs) up to 12. Analytic and FEM results match well and show the speed dependency of the conical modes, demonstrating the influence of rotor dynamics. All three rigid body modes are crossed already by the first EO in the operating range of the SBMs. Therefore this modes are especially relevant for the SBMs control system since they are excited by the unbalance forces which have an EO of one. With the moments of inertia of the present rotor leading to a rotordynamically long rotor (in contrast to a disk shape), the rotational speed dependence of the whirl resonances is relatively low. At speeds above 5500 rpm supercritical operation with respect to the rigid body modes is achieved.

### C. Rotor Bending Modes

The rotor bending modes are analysed by means of 3D-FEM. The FEM rotor model of **Fig. 10c)** was used. The FEM results are shown in **Fig. 12**. Given the expected relevant frequency range of up to 4000 Hz defined by the speed operating range and expected relevant EOs of up to 12, the first two bending modes were computed. Both bending modes show both a forward (i.e. in rotation direction) and a backward whirl speed dependent resonance frequency. In **Fig. 12c)**, the mode shapes of the first bending mode are shown. The rotor magnets at both rotor ends are not at a node, therefore the magnets also radially move within this mode. **Fig. 12b)** shows the second bending mode. In this mode, the magnets are not at a node as well. A Campbell diagram with the FEM results of the resonance frequencies and intersecting EO are presented in **Fig. 12a)**. It can be concluded, that only higher order excitations cross and therefore can excite the rotor bending modes.

The present system was found to operate sub-critically with respect to the rotor bending modes, i.e. the first EO does

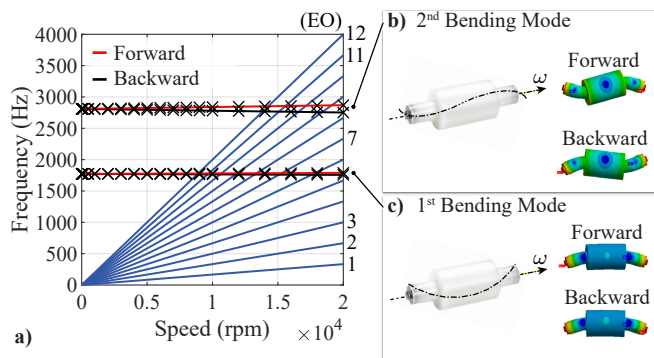


**Fig. 12:** This figure shows the bending modes of the test-rotor. **a)** Campbell diagram with 3D FEM rotor model results of the bending modes. The excitation orders 1-12 (EO) are indicated as well. The principal motion and corresponding FEM results for the displacement pattern from the initial position (blue=low, red=high) for the second **b)** and first **c)** bending mode are shown.

not intersect these modes. Nevertheless higher order EO can principally excite them.

#### D. Experimental Verification

The control structure shown in **Fig. 9** was implemented on the control test-platform presented in **Fig. 8**. The system resonance frequencies due to rigid body modes were successfully passed, showing the successful operation of the force rejection. The maximum speed of the control test-system of 20'000 rpm was successfully reached without incidences in the ramp up. This means that possible higher order excitations did not noticeably excite the bending resonances of the rotor. The higher order excitations in slotless SBMs are expected to be smaller than in the control test-system SBMs with temple architecture due to the missing stator teeth. It seems therefore very promising that for the UCF SBM concept, the control system will work well. The control system as such could therefore successfully be verified. It seems beneficial, if ultracentrifuge rotors are designed stiff enough, such that their bending modes are not excited for EOs equal to one during operation or ramp-up respectively.

### V. CONCLUSION & OUTLOOK

A novel magnetically double self-bearing drive system concept for ultracentrifugation with motor opening functionality and performance towards 100'000 rpm and 200'000 g was presented. The ultracentrifuge application goals, requirements and resulting challenges were identified and compared to other self-bearing drive system applications. The feasibility of the presented concept regarding centrifugation performance, power consumption and mechanical integrity was successfully demonstrated. Slotless self-bearing motors with distributed windings and a pole pair number equal to one were identified as an ideal topology for the ultracentrifuge application, enabling a unique motor opening mechanism, allowing for easy access and removal of the ultracentrifuge rotor. A prototype self-bearing motor and corresponding test system was presented. A control structure for the double self-bearing

drive system was proposed. System resonance modes were unveiled analytically and with 3D-FEM. The control system was implemented on an established control test-platform and successfully operated to the platforms speed-limit. As future work, the further commissioning of the ultracentrifuge self-bearing motor prototype and system-level integration and testing are targeted.

### REFERENCES

- [1] M. Konrath, J. Gorenflo, N. Hübner and H. Nirschl, "Application of magnetic bearing technology in high-speed centrifugation," *Chemical Engineering Science*, vol. 147, pp. 65-73, 2016.
- [2] W. Gruber, W. Bauer, D. Wetsch, B. Klammer and N. Kurita "Implementation of a Bearingless Axial-Force/Torque Motor Fan with Flex-PCB Windings," *Proc. of IEEE International Electric Machines & Drives Conference (IEMDC)*, pp. 179-184, 2019.
- [3] C. Zwysig, T. Baumgartner, J.W. Kolar "High-Speed Magnetically Levitated Reaction Wheel Demonstrator," *Proc. of International Power Electronics Conference (IPEC - ECCE ASIA)*, pp. 1707-1714, 2014
- [4] A. Tüysüz, T. Achtnich, C. Zwysig and J.W. Kolar "A 300'000-r/min Magnetically Levitated Reaction Wheel Demonstrator," *IEEE Transactions on Industrial Electronics*, vol. 66, no. 8, pp. 6404-6407, 2018.
- [5] H. Mohr and A. Völkl, "Ultracentrifugation," *eLS*, 2017.
- [6] E. Bilgen and R. Boulos, "Functional Dependence of Torque Coefficient of Coaxial Cylinders on Gap Width and Reynolds Numbers," *ASME. J. Fluids Eng.*, vol. 95, no. 1, pp. 122-126, 1973.
- [7] P.R.N. Childs, "Rotating flow," *Elsevier*, 2010.
- [8] S. Tarleton and R. Wakeman "Solid/liquid separation: scale-up of industrial equipment," *Elsevier*, 2011.
- [9] R. Larsonneur "Design and control of active magnetic bearing systems for high speed rotation," *Diss. ETH Zurich*, pp. 12-15, 1990.
- [10] I. Szabó "Höhere technische Mechanik," *Springer*, pp. 165-166, 2013.
- [11] R. Rennert, E. Kullig, M. Vormwald, A. Esderts and D. Siegele "FKM-Richtlinie: Rechnerischer Festigkeitsnachweis für Maschinenbauteile," *Forschungskuratorium Maschinenbau (FKM)*, 2012.
- [12] P. Peralta, D.M. Araujo and Y. Perriard "Design of Compact Bearingless Disc Drive Systems," *IEEE Transactions on Industry Applications*, vol. 56, no. 5, pp. 4870-4881, 2020.
- [13] D. Steinert, T. Nussbaumer and J.W. Kolar "Slotless Bearingless Disk Drive for High-Speed and High-Purity Applications," *IEEE Transactions on Industrial Electronics*, vol. 61, no. 11, pp. 5974-5986, 2014.
- [14] P. Puentener, M. Schuck, D. Steinert and J.W. Kolar "Comparison of Bearingless Slice Motor Topologies for Pump Applications," *Proc. of International Electric Machines & Drives Conference (IEMDC)*, pp. 9-16, 2019.
- [15] D. Steinert, T. Nussbaumer, J.W. Kolar "Topology Evaluation of Slotless Bearingless Motors with Toroidal Windings," *Proc. of International Power Electronics Conference (IPEC - ECCE ASIA)*, pp. 975-981, 2014.
- [16] R. Schoeb and N. Barletta "Principle and Application of a Bearingless Slice Motor," *JSME International Journal Series C Mechanical Systems, Machine Elements and Manufacturing*, vol. 40, no. 4, pp. 593-594, 1997.
- [17] G. Schweitzer and E.H. Maslen "Magnetic Bearings," *Springer*, pp. 217, 2009.
- [18] A. Preumont, "Twelve Lectures on Structural Dynamics," *Springer*, pp. 217, 2013,